Light Curve Analysis Using Wavelets

Andrew D. Dianetti* and John L. Crassidis†

University at Buffalo, State University of New York, Amherst, NY 14260-4400

A method is presented that uses wavelet decomposition in the analysis of light curves. Wavelet decomposition allows the frequency of a signal to be determined over time, and when applied to the light curve reflected by a space object, is used to determine the angular rate over time. This allows for detection in changes of the spacecraft's attitude state. Several cases of attitude maneuvers are presented, and the wavelet decomposition process is demonstrated using simulated and experimentally obtained data. The process is also applied to real observations of the GOES-16 satellite. Wavelets allow for better temporal and frequency resolution compared to traditional frequency-domain methods such as the Short-Time Fourier Transform.

I. Introduction

Light curves, or the time-history of the intensity of reflected light, can be used to estimate attributes of Resident Space Objects (RSOs). One such attribute of interest is the spacecraft's attitude state. Traditional estimation methods such as Kalman Filtering have been used to estimate attitude from light curve measurements [1]. However, such an approach requires knowledge of the object's shape, as well as an assumed reflectance model. This is necessary for attitude observability [2]. In reality, the shape of the object may not be known. Simultaneous shape and attitude estimation has been demonstrated using filtering methods [3][4], but such methods require assumptions about the model. If these assumptions do not describe the actual system, such methods are unlikely to perform well. Additionally, in some cases, light curves may not provide sufficient information to enable precise attitude determination using these methods [5]. Therefore, there is a desire to employ non-model-based methods in determining attitude information from light curves.

The light curve is well-suited to determining the rotation rate of the spacecraft, as such rotation produces a periodic light curve. Detecting changes in rotational states is useful in detecting anomalies and potential activities of space objects. Determining the rotational rate and being able to detect changes in the rotational state of a space object is an area of interest in Space Situational Awareness (SSA).

Wavelet decomposition is a method that is demonstrated to allow for identification of such rotational rates and changes in the rotational state of a space object using the light curve, especially in real-time situations. This paper will present an overview of the wavelet decomposition, discuss advantages over traditional frequency-domain methods, and present results for different scenarios using both simulated and actual data.

II. Fourier Transform

Traditional frequency-domain methods, such as the Fourier Transform, are not well-suited for real-time applications. The Fast Fourier Transform (FFT) does not capture time-varying behavior, only aggregate behavior from the sampling period. Figure 1 shows a FFT of a tumbling object with a constant rotation rate, and the same object subjected to a stabilization maneuver. It is seen that this method does not detect the stabilization maneuver, and that when the stabilization maneuver is included, the dominant frequency does not correspond to the rotational rate. Such a method does not provide any information about events that occur during the sampled window.

*Graduate Student, Department of Mechanical & Aerospace Engineering. Email: andrewdi@buffalo.edu. Student Member AIAA.

†CUBRC Professor in Space Situational Awareness, Department of Mechanical & Aerospace Engineering. Email: johnc@buffalo.edu. Fellow AIAA.

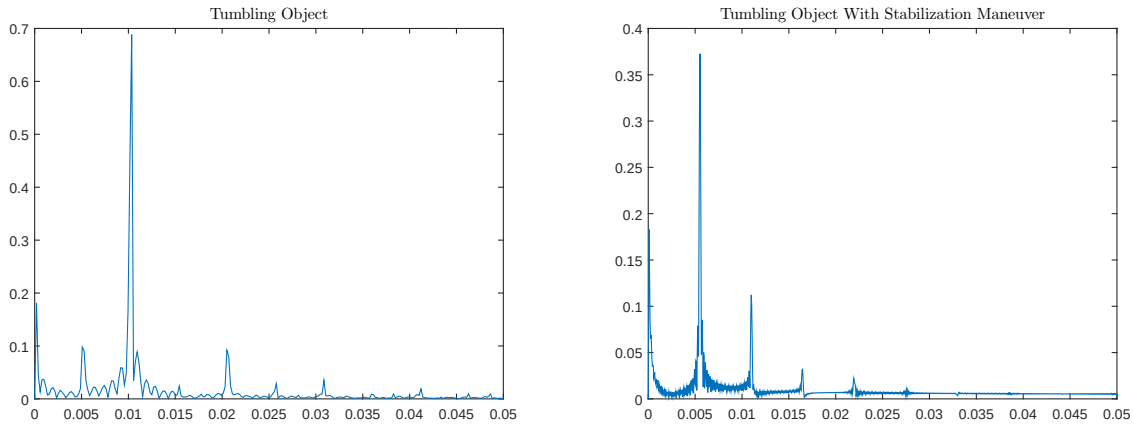

Figure 1. Fast Fourier Transform of constant tumbling object (left) and tumbling object with stabilization behavior (right).

An alternative method that allows application in quasi-real time is the Short-Time Fourier Transform (STFT), which uses a moving window to compute frequency components over time. However, in this case, the window size is fixed. This limits the observable frequencies to the Nyquist limit − or half the sampling frequency. Wavelets, however, allow for variable window sizes for analyzing different frequency components.

III. Wavelet Overview

While the essence of the Fourier Transform is to fit periodic sine and cosine components of different frequencies to the data, wavelets are a class of functions that are fit to the data by scaling and translation in time. This scaling function is time dependent. There exist many different classifications of wavelets, which have different wavelet and scaling functions, but for each class, the shape of these functions remains unchanged. Only the time extension is changed. The wavelet function can essentially be thought of as a band-pass filter, where the scaling function controls the bandwidth. An example of the Symlet-6 wavelet is shown in Figure 2. There exist many different classes of wavelets, some of which have many wavelets that

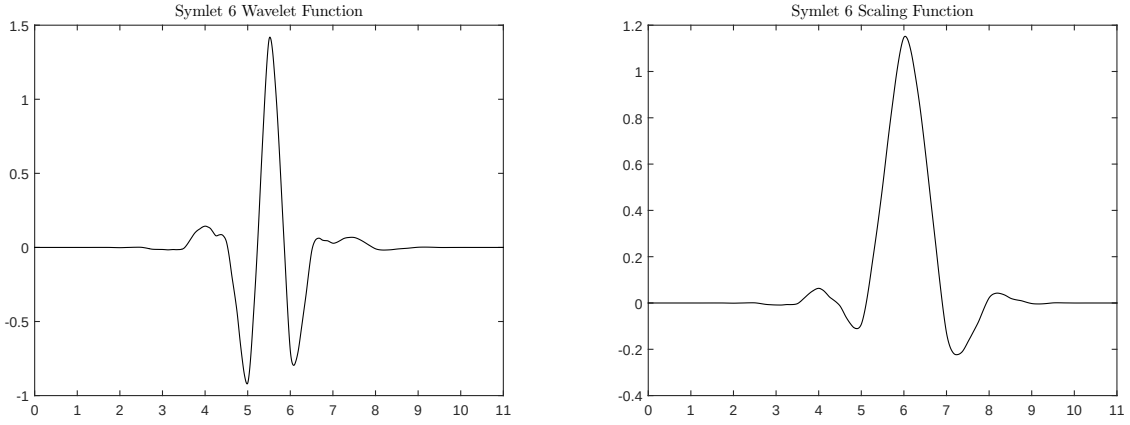

Figure 2. Symlet-6 Wavelet

make up the class. An example of the Haar wavelet, which has a constant scaling function of 1, is shown in Figure 3 and wavelets with in the Daubeuchies class are shown in Figure 4.

If ψ is denoted as the "mother wavelet", then the signal can be represented as a composition of the "child

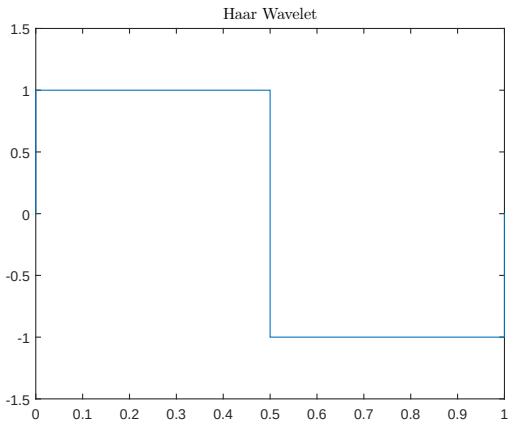

]

Figure 3. Haar Wavelet

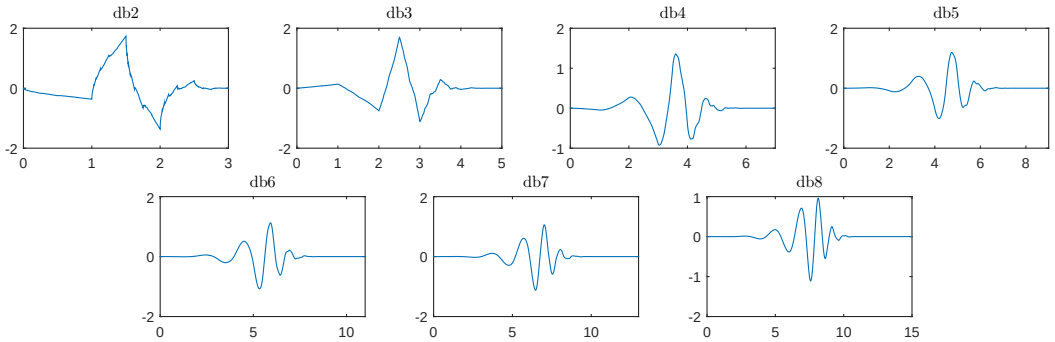

Figure 4. Wavelets within Daubeuchies class

wavelets"

$$\psi_{j,k}(t) = \frac{1}{\sqrt{s_0^j}}\psi\left(\frac{t - k\tau_0 s_0^j}{s_0^j}\right) \tag{1}$$

where j and k are positive integer indices, s_0 is a positive real number that defines the scale, and τ_0 is any real number that defines the shift. If $s_0 = 2$ and τ_0 are chosen, this results in dyadic sampling on both the frequency and time axes. Then, the original signal $f(t)$ is constituted of the scaling function γ and the child wavelets:

$$f(t) = \sum_{j,k} \gamma(j,k)\psi_{j,k}(t) \tag{2}$$

In discrete time, the wavelet transform can be treated as a set of high-pass and low-pass filters, without the need to analytically determine the wavelets. This is a process known as wavelet decomposition. With each filter that is applied, each point ends up being sampled twice, so then we subsample by a factor of two, as shown in Figure 5. If only the wavelet functions ϕ were available, it would require an infinite number of filters to capture a frequency of zero, using the method shown in Figure 5. The scaling function γ is thus used to expand the spectrum covered by each wavelet as shown in Figure 6. With this decomposition, as the frequency decreases, the frequency resolution increases. Likewise, as the requency increases, the time resolution increases. The limit of the time and frequency resolutions is given by

$$\Delta t \Delta f >= \frac{1}{4\pi} \tag{3}$$

This is notably better than the Nyquist limit of the STFT. A plot of frequency vs. time with the limiting resolution for the STFT and the wavelet transform is shown in Figure 7. It is seen that at the same frequency

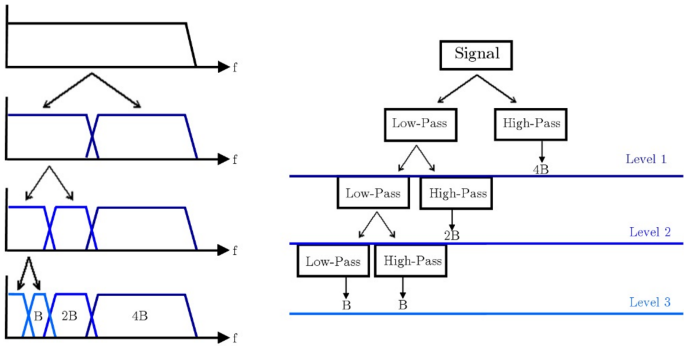

Figure 5. Wavelet transform process. Frequency spectrum decomposition shown on left, wavelet tree decomposition shown on right.

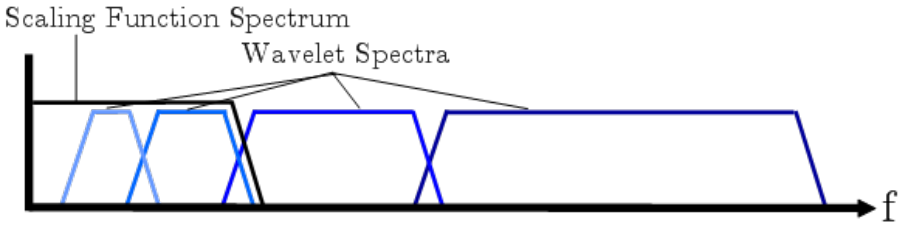

Figure 6. Frequency spectrum when scaling functions are used to expand wavelet spectra

resolution, the wavelet transform provides better time resolution of high frequencies, and likewise, at the same time resolution, provides better frequency resolution for low frequencies.

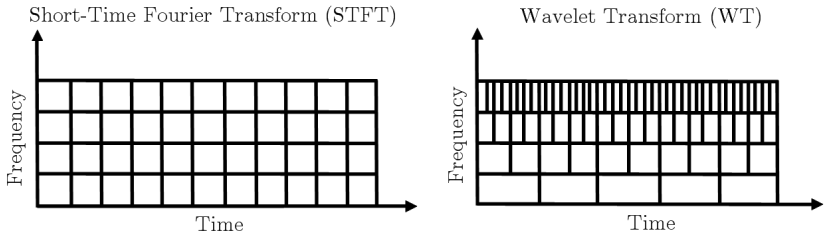

Figure 7. Frequency vs. time resolution for STFT and Wavelet Transform

IV. Light Curve Results

As noted in the prior section, the wavelet transform provides frequency and temporal resolution, e.g. the frequency over time. If it is assumed that variations in brightness of an observed object are due to changes in its attitude, then the wavelet decomposition can provide angular velocity over time.

A. Simulated Data

Data for a tumbling RSO is sumulated with a rotational rate of 3.6 deg/s, or 0.01 Hz. A light curve is generated using the Bidirectional Reflectance Distribution Function (BRDF) developed by Ashikmin and Shirley [6]. This reflection model is briefly summarized below. The reflection geometry is shown in Figure 8. Each facet has a set of three basis vectors ($\boldsymbol{u}_n^B$, $\boldsymbol{u}_u^B$, $\boldsymbol{u}_v^B$). The unit vector $\boldsymbol{u}_n^B$ points in the direction of the outward normal to the facet, which is the same vector used in the SRP model, and the vectors $\boldsymbol{u}_u^B$ and

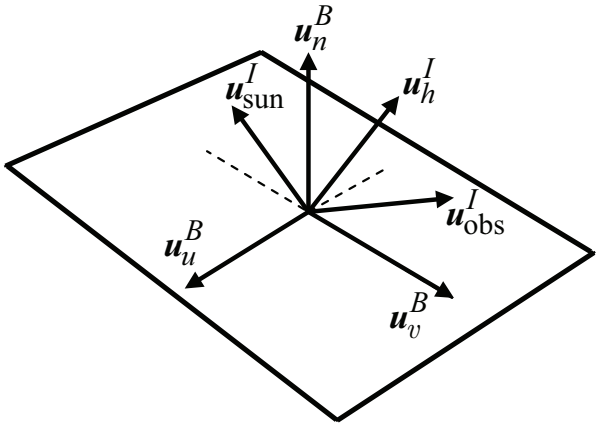

Figure 8. Reflection Geometry

$\boldsymbol{u}_v^B$ are in the plane of the facet. The object is assumed to be a rigid body so that the unit vectors $\boldsymbol{u}_n^B$, $\boldsymbol{u}_u^B$ and $\boldsymbol{u}_v^B$ do not change since they are expressed in the body frame. The vector $\boldsymbol{u}_h^I$ is the normalized half vector between $\boldsymbol{u}_{\text{sun}}^I$ and the observation unit vector $\boldsymbol{u}_{\text{obs}}^I$. The observation vector is usually given in body coordinates with $\boldsymbol{u}_{\text{obs}}^B = A(\boldsymbol{q})\boldsymbol{u}_{\text{obs}}^I$.

The BRDF at any point on the surface is a function of two directions, the direction from which the light source originates and the direction from which the scattered light leaves the observed surface. The model in Ref. [6] decomposes the BRDF into a specular component and a diffuse component. The two terms sum to give the total BRDF:

$$\rho_{\text{total},\,i} = \rho_{\text{spec},\,i} + \rho_{\text{diff},\,i} \tag{4}$$

The diffuse component represents light that is scattered equally in all directions (Lambertian) and the specular component represents light that is concentrated about some direction (mirror-like). Reference [6] develops a model for continuous arbitrary surfaces but simplifies for flat surfaces. This simplified model is employed in this work as shape models are considered to consist of a finite number of flat facets. Therefore the total observed brightness of an object becomes the sum of the contribution from each facet.

Under the flat facet assumption the specular term of the BRDF becomes

$$\rho_{\text{spec},\,i} = \frac{\sqrt{(n_u+1)\,(n_v+1)}}{8\pi} \frac{\left(\boldsymbol{u}_{n,\,i}^I \cdot \boldsymbol{u}_h^I\right) \left\{ \frac{n_u(\boldsymbol{u}_h^I \cdot \boldsymbol{u}_{u,\,i}^I)^2 + n_v\left[1-(\boldsymbol{u}_h^I \cdot \boldsymbol{u}_{v,\,i}^I)^2\right]}{\left(1-\left[\boldsymbol{u}_{n,\,i}^I \cdot \boldsymbol{u}_{h,\,j}\right]\right)^2} \right\}}{\boldsymbol{u}_{n,\,i}^I \cdot \boldsymbol{u}_{\text{sun}}^I + \boldsymbol{u}_{n,\,i}^I \cdot \boldsymbol{u}_{\text{obs}}^I - (\boldsymbol{u}_{n,\,i}^I \cdot \boldsymbol{u}_{\text{sun}}^I)(\boldsymbol{u}_{n,\,i}^I \cdot \boldsymbol{u}_{\text{obs}}^I)} F_{\text{reflect},\,i} \tag{5}$$

where j indicates the j^{th} observer, and the Fresnel reflectance is given by

$$F_{\text{reflect},\,i} = R_{\text{spec},\,i} + (1 - R_{\text{spec}}\,(i)) \left(1 - \boldsymbol{u}_{\text{sun}}^I \cdot \boldsymbol{u}_{h,\,i}^I\right)^5 \tag{6}$$

The parameters of the Phong model that dictate the direction (locally horizontal or vertical) distribution of the specular terms are n_u and n_v. The diffuse term of the BRDF is

$$\rho_{\text{diff},\,i} = \left(\frac{28 R_{\text{diff},\,i}}{23\pi}\right)(1 - R_{\text{spec},\,i}) \left[1 - \left(1 - \frac{\boldsymbol{u}_n^I(i) \cdot \boldsymbol{u}_{\text{sun}}^I}{2}\right)^5\right] \left[1 - \left(1 - \frac{\boldsymbol{u}_n^I(i) \cdot \boldsymbol{u}_{\text{obs}}^I}{2}\right)^5\right] \tag{7}$$

The apparent magnitude of the object is the result of sunlight reflecting off of its surfaces along the line-of-sight to an observer. First, the fraction of visible sunlight that strikes an object (and not absorbed) is computed by

$$F_{\text{sun},\,i} = C_{\text{sun,vis}}\, \rho_{\text{total},\,i} \left(\boldsymbol{u}_{n,\,i}^I \cdot \boldsymbol{u}_{\text{sun}}^I\right) \tag{8}$$

where $C_{\text{sun,vis}} = 455$ W/m^2 is the power per square meter impinging on a given object due to visible light striking the surface. If either the angle between the surface normal and the observer's direction or the angle

between the surface normal and Sun direction is greater than $\pi/2$ then there is no light reflected toward the observer. If this is the case then the fraction of visible light is set to $F_{\text{sun},\,i} = 0$.

The fraction of sunlight that strikes a surface that is reflected given by

$$F_{\text{obs},\,i} = \frac{F_{\text{sun},\,i}\, A_{\text{proj},\,i}\, \left(\mathbf{u}^I_{n,\,i} \cdot \mathbf{u}^I_{\text{obs}}\right)}{d^2} \tag{9}$$

where d is the distance from the observer to the object. The reflected light is now used to compute the apparent brightness magnitude, which is measured by an observer through

$$m_{\text{app}} = -26.7 - 2.5\log_{10}\left|\sum_{i=1}^{N} \frac{F_{\text{obs},\,i}}{C_{\text{sun,vis}}}\right| \tag{10}$$

where -26.7 is the apparent magnitude of the Sun, and N is the total number of facets.

A Symlet-6 wavelet decomposition is used, and the rotational rate is identified by the wavelet transformation, as shown in Figure 9.

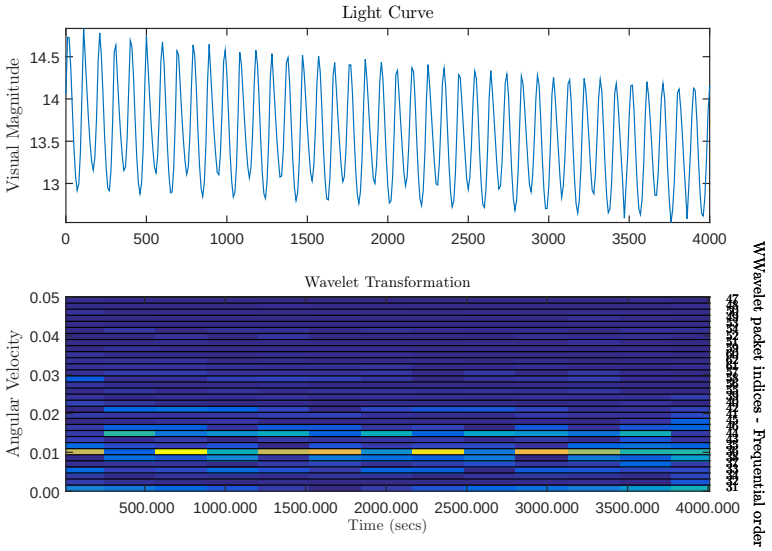

Figure 9. Wavelet decomposition for light curve of tumbling object.

Wavelets are seen to detect changes in object behavior. Different cases have unique wavelet signatures. For example, Figure 10 shows the wavelet decomposition of the light curve of an object with a constant torque applied to it. The corresponding linear increase in angular velocity is clearly seen. Figure 11 shows

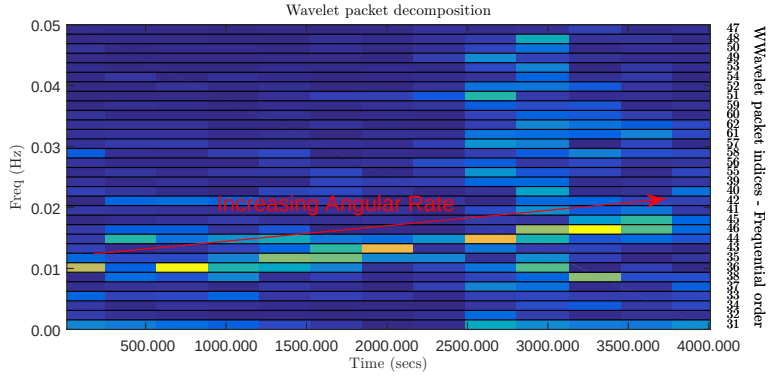

Figure 10. Wavelet decomposition of object with constant applied torque, clearly showing increase in angular rate.

the case of a tumbling object that undergoes a stabilization maneuver. It is clearly seen that the wavelet decomposition correctly identifies the angular velocity before and after the maneuver, as well as the time at which the maneuver occurred. This shows the power of the wavelet decomposition in detecting state changes and anomalies. The case of a stabilized RSO that undergoes a re-pointing maneuver is also considered,

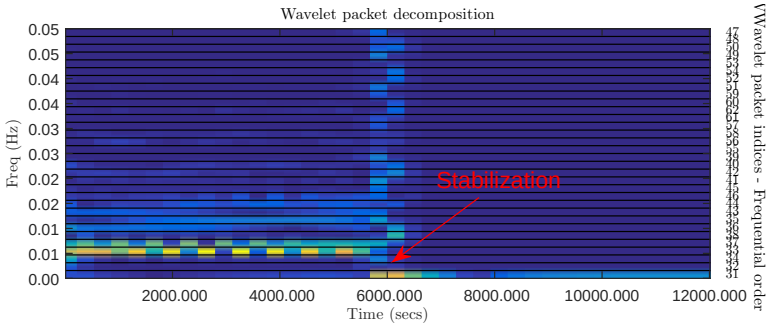

Figure 11. Wavelet decomposition of tumbling object that undergoes a stabilization maneuver.

shown in Figure 12. Although there is no periodicity in the signal, there is a change in the reflected light magnitude that occurs during the time of the maneuver. This changes the wavelet decomposition at this point, essentially changing the shape of the light curve. This changes the wavelet decomposition at this point, which is visible as an increased magnitude of zero-frequency signal. Thus, even in the absence of periodicity, wavelets can detect changes in state that produce changes in the light curve.

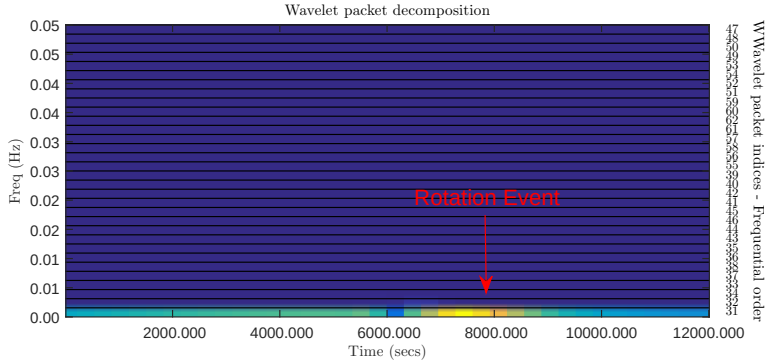

Figure 12. Wavelet decomposition of stabilized RSO with re-pointing maneuver

B. Experimental Data

There is a desire to experimentally measure light curves in validation of characterization algorithms. Since RSO observations with known truth data can often be difficult to acquire, a laboratory set up has been developed to measure the light curve of a rotating object. Objects are placed on a rotating platform and illuminated with a 1065 lumen LED bulb, which is focused onto the object to minimize ambient illumination. A PCO Pixelfly USB camera is used to acquire images of the object. This setup is depicted in Figure 13. Images are taken, and for each image the region corresponding to the object is isolated and the total intensity of the region is computed. Figure 14 shows a sequence of these images and the isolation of the region corresponding to the object. The same cases as in the simulated data are run experimentally. Figure 15 shows the increasing angular rate case, Figure 16 shows the stabilization maneuver, and Figure 17 shows the re-pointing maneuver. It is seen in these figures that the wavelet decomposition identifies the same behavior as the simulated cases.

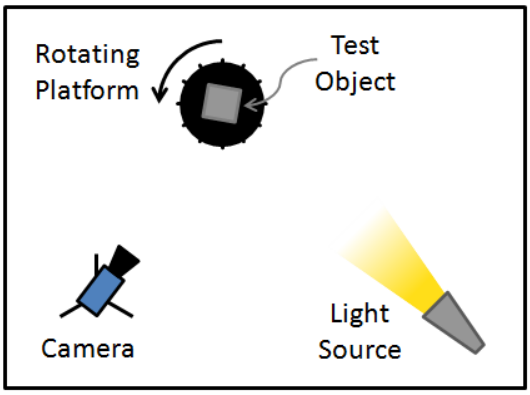

Figure 13. Experimental setup

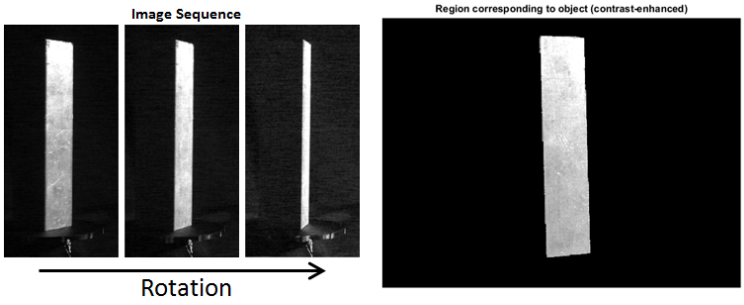

Figure 14. Images taken by experimental setup. Left side shows rotation sequence, right side shows isolation of object region.

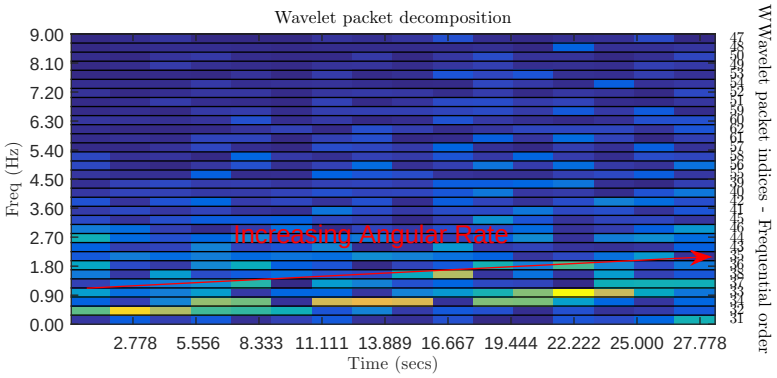

Figure 15. Wavelet decomposition for experimental increasing angular rate case

C. RSO Observation Data

The wavelet analysis is now applied to an observation of the GOES-16 spacecraft taken during a series of maneuvers. GOES-16 is a geostationary satellite that is nominally earth-pointing, which means that periodic behavior will not be observed over the course of one night. The light curve and wavelet analysis are shown in Figure 18. There are three notable maneuver events that are visible in the light curve − two jumps and one period of oscillatory behavior. All of these are clearly identified in the wavelet analysis.

It is also seen that above a magnitude of approximately $m_{app} = 12.5$, the data becomes quite noisy. This noise causes an increase in the low-frequency component of the wavelet analysis, even though there is no identifiable behavior occurring within the light curve. This underscores the need for low-noise data, or further development of algorithms to handle such noise.

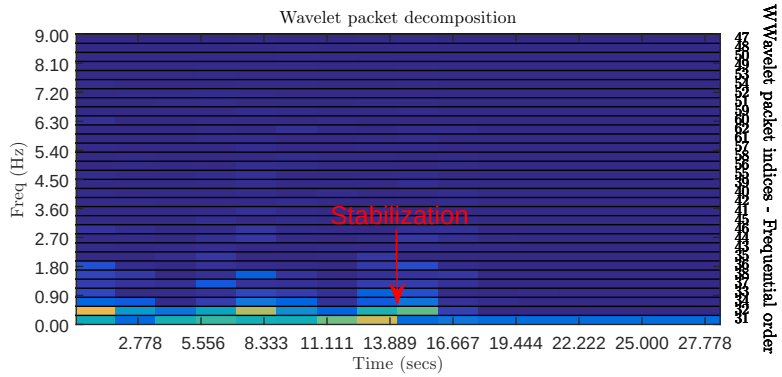

Figure 16. Wavelet decomposition for experimental stabilization case

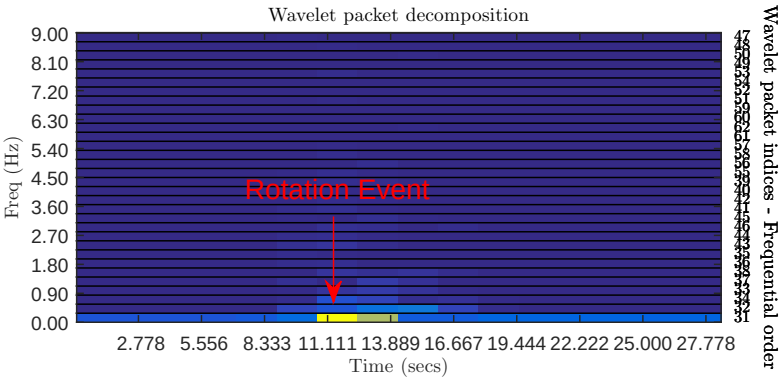

Figure 17. Wavelet decomposition for experimental re-pointing case

V. Future Work

In the current implementation, glint events present issues with the wavelet analysis. Glint events are short events where the magnitude of reflected light becomes substantially brighter due to specular reflection. If this occurs in during periodic diffuse reflection, the large magnitude of the glint event causes the wavelet decomposition to include higher frequency components, as shown in Figure 19. Future work will involve research into methods to mitigate this effect.

VI. Conclusion

Wavelet analysis has been demonstrated to be a promising method for detection of changes in RSO attitude state using light curves. Several different cases are presented using both simulated and experimentally obtained light curve data. These cases produce unique signatures in the frequency vs. time plots generated using wavelet analysis. Additionally, the wavelet analysis was able to successfully identify maneuvers from a light curve taken of the GOES-16 satellite. Wavelet analysis is a non-model-based approach, and could be a promising method when such an approach is desired.

References

[1]Wetterer, C. J. and Jah, M., "Attitude Estimation from Light Curves," *Journal of Guidance, Control and Dynamics*, Vol. 32, No. 5, Sept.-Oct. 2009, pp. 1648–1651, doi:10.2514/1.44254.

[2]Hinks, J., Linares, R., and Crassidis, J., "Attitude Observability from Light Curve Measurements," *AIAA Guidance, Navigation, and Control Conference*, AIAA, Reston, VA, Aug. 2013, doi:10.2514/6.2013-5005.

[3]Wetterer, C. J., Hunt, B., Hamada, C., Crassidis, J. L., and Kervin, P., "Shape, Surface Parameter, and Attitude Profile Estimation Using a Multiple Hypothesis Unscented Kalman Filter," *AAS/AIAA Space Flight Mechanics Meeting*, AAS, Springfield, VA, Jan. 2014, AAS Paper #14-303.

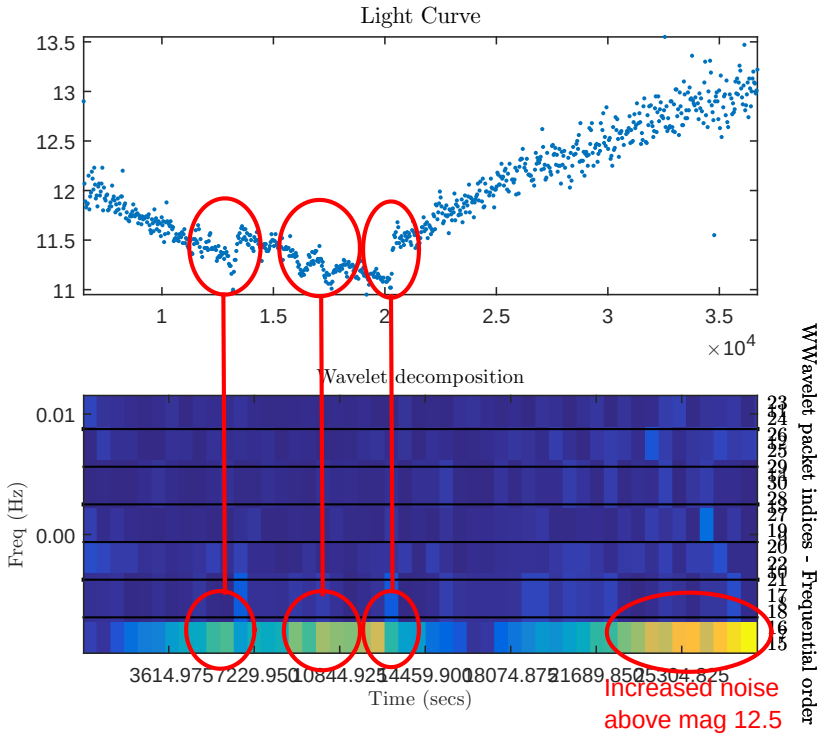

Figure 18. GOES-16 light curve (top) and wavelet analysis (bottom)

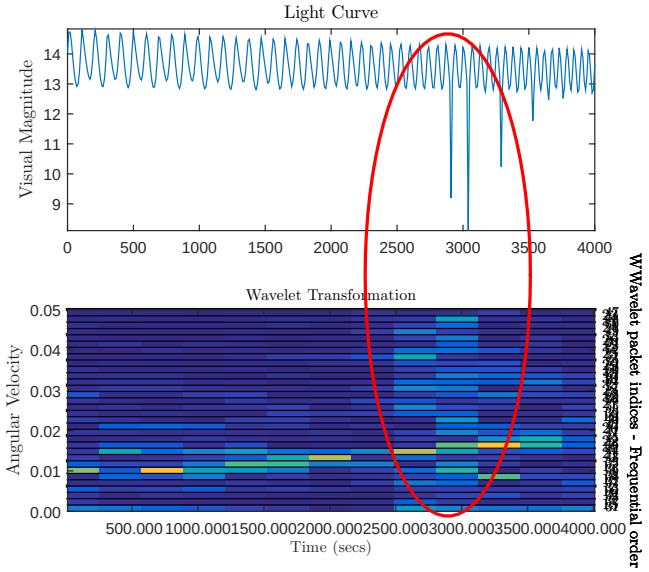

Figure 19. Wavelet decomposition of light curve including glint events

[4]Wetterer, C. J., Chow, C. C., Crassidis, J. L., and Linares, R., "Simultaneous Position Velocity, Attitude, Angular Rates, and Surface Parameter Estimation Using Astrometric and Photometric Observations," *16th International Conference on Information Fusion*, IEEE, Piscataway, NJ, July 2013, pp. 997–1004, doi:10.2514/6.2013-5005.

[5]Dianetti, A., Weisman, R., and Crassidis, J., "Observability Analysis for Improved Space Object Characterization," *Journal of Guidance, Control, and Dynamics*, 2017, doi:10.2514/1.G002229.

[6]Ashikmin, M. and Shirley, P., "An Anisotropic Phong Light Reflection Model," Tech. rep., University of Utah, Salt Lake City, UT, 2000.